THE JOURNAL OF PHYSICAL CHEMISTRY B

pubs.acs.org/JPCB Article

Mixed Quantum Classical Simulations of Charge-Transfer Dynamics in a Model Light-Harvesting Complex. I. Charge-Transfer Dynamics

Published as part of The Journal of Physical Chemistry virtual special issue "Peter J. Rossky Festschrift".

Kush Patel and Eric R. Bittner*

Cite This: *J. Phys. Chem. B* 2020, 124, 2149–2157 Read Online

ACCESS | Metrics & More | Article Recommendations

ABSTRACT: We develop here a mixed quantum mechanical/molecular dynamics model to investigate charge-transfer dynamics in a set of large organic donor–bridge–acceptor triad molecules. Specifically, we are interested in the differences in electron and nuclear behavior relating to small changes in the molecular makeup of carotenoid–porphyrin–fullerene triads. Our model approximates excitation energies on the order of 1.9 eV which agree with absorption spectra for these triads and isolated porphyrins. Using electron population analysis, we monitor charge migration to the acceptor in time. Approximations of the charge transfer rates reveal ultrafast (picosecond scale) electron dynamics consistent with experimental literature.

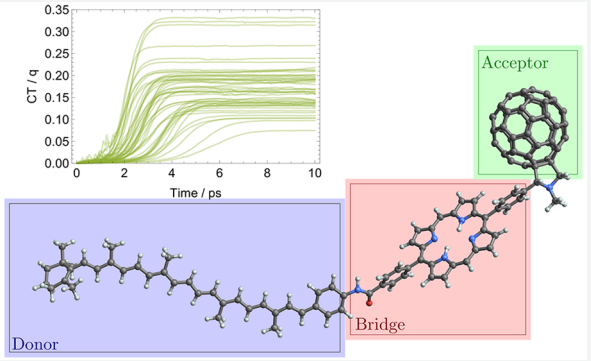

INTRODUCTION

Nature has been using light for billions of years to generate chemical energy for splitting water, and significant effort has gone into the characterization of such biomimetic systems. In particular, donor–bridge–acceptor (DBA) triads composed of highly conjugated subunits readily undergo intramolecular rapid charge transfer and have slow electron/hole recombination rates, leading to long-lived charge-transfer states and a quantum yield of near unity. These processes occur in a single molecular framework, and it is for these reasons that DBA triads provide an ideal system of study.

We consider here a series of model systems that mimic the light-harvesting process that initiates the photosynthetic processes in a biological system. Moore and co-workers have experimentally investigated a wide array of dyads (donor/acceptor) and triads (donor/bridge/acceptor) that mimic the photosynthetic processes of bacterial reaction centers.[1−9] They have shown that porphyrin–quinone and porphyrin–C_{60} dyad systems can maintain charge separation for time scales up to hundreds of picoseconds.[3,6] The addition of a carotenoid polyene moiety increases this lifetime (in some cases by 3 orders of magnitude) by increasing the physical separation of the charges. This claim is evidenced by a readily detectable transient absorption band of the carotenoid radical cation.[10]

Triadic systems of this design undergo a multistep electron transfer process. First, the chromophore bridge (porphyrin) is photoexcited into a singlet excited state.

$$C{-}P^{*}{-}C_{60} \xrightarrow{k_e} C{-}P^{+}{-}C_{60}^{-} \quad (1)$$

Experimental studies of the formation of the first CT state in carotenoid–porphyrin–fullerene (CPF) triads indicate that the quantum yield for this process lies around $\Phi > 0.85$. This is followed by electron transfer to the acceptor moiety (k_e) which is driven by the energetic offset between the exciton and first charge-transfer state $CP^{+}C_{60}^{-}$.

$$C{-}P^{+}{-}C_{60} \xrightarrow{k_h} C^{+}{-}P{-}C_{60}^{-} \quad (2)$$

This state can undergo a decay process into the carotenoid triplet state[11] and finally relax down to the ground state. Incidentally, this triplet state, which provides photoprotection from singlet oxygen, is not seen in many other biomimetic materials but is seen in natural photosynthetic systems.[6]

Charge-transfer rates depend on the molecular system. It is surprising, however, just how sensitive they are to seemingly minor changes in moiety linkers and even side substituent groups. For example, in triads with donor–bridge units linked by an amide group, reversal of the amide direction changes the

Received: January 8, 2020
Revised: February 19, 2020
Published: March 2, 2020

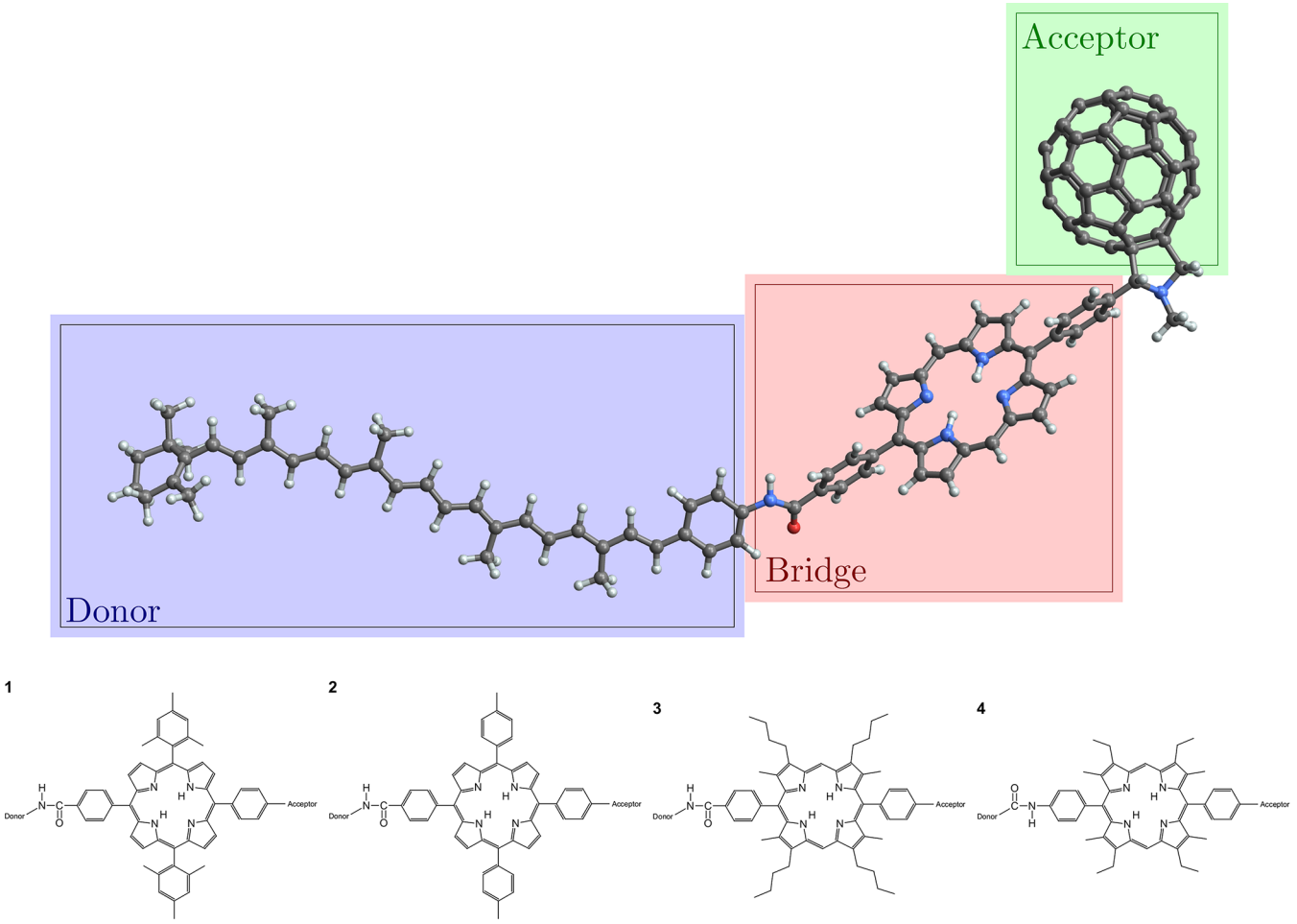

Figure 1. (Top) Basic construction of the donor−bridge−acceptor triad composed of a carotenoid donor (blue), porphyrin bridge (red), and fullerene derivative acceptor (green). Alternative structures include addition of side groups to the porphyrin in β or *meso* positions, increasing the distance between subunits via methylene units or a different fullerene derivative. (Bottom) The bridging moieties differentiate the molecules.

rate of formation of the final CT state by a factor of ∼30.[3] This directional bias is supported by a number of studies on the rectification behavior of small molecules and linkers[12−14] and primarily attributed to electronic asymmetry.

The choice of side groups on the bridge can affect the electronic coupling between the bridge and acceptor. In several CPF triads studied, porphyrin bridges are linked to the fullerene acceptor via an aryl group. Fluctuations of the dihedral angle between this linker and porphyrin not only modulate the electronic coupling to the acceptor but also consequently affect the energy difference between excited and charge-transfer states. Large aliphatic side groups in the β positions sterically hinder the accessible angles the linker can sample. Small dihedral angles increase the p_z orbital overlap where angles closer to $\pi/2$ close the overlap. Therefore, bridges with smaller side groups should allow better electronic overlap and result in faster CT rates. However, experimental measurements prove otherwise: triads with aliphatic groups proved an order of magnitude faster.[5,9] The absorption spectrum of the triads is remarkably close to a linear combination of spectra of the individual moieties,[5,15] indicating that when covalently linked the moieties are nearly electronically independent; the electronic structure is only weakly perturbed in the triad form. Bahr and co-workers argue, in the frame of Marcus theory, that the thermodynamic driving force, ΔG, has a much more significant effect on the CT rate.

Rozzi and co-workers have combined experimental and theoretical techniques on a study of one CPF triad.[15] Their experimental work studies the triad in Figure 1 with addition of mesitylene molecules at the porphyrin *meso* positions. Their theoretical work considers only the basic construction of the triad. In this work, they claimed coherent ultrafast charge transfer occurs at the sub-100 fs scale. Differential transmission spectra showed the rise of a few bands following system photoexcitation in the neighborhood of 550 nm. Each of these bands exhibited oscillatory behavior in intensity with a period of about 30 fs.

A time-dependent density functional theory (TDDFT) excited-state dynamics simulation was performed on a similarly structured triad.[16] By spatially integrating the electron density around the fullerene moiety, they measured the charging of the acceptor in time. A full electron of charge migrated to the fullerene with the charging shape also having some oscillatory behavior (roughly 30 fs period). As this is close to the conjugated carbon−carbon bond stretching period, they concluded that such nuclear vibrations are fundamental to CT. Moreover, excited-state electronic flow through the system can be effectively suppressed by freezing subsets of nuclei within the DBA system.

It is important to note that ref 15 only considered the results of a *single trajectory* which may not represent the actual CT dynamics within these triads. Surprisingly, while the computa-

https://dx.doi.org/10.1021/acs.jpcb.0c00202
J. Phys. Chem. B 2020, 124, 2149−2157

tional work offers insight into the experimental results, the molecular structure presented in the supplementary media of simulations does not reflect the molecule presented for their experimental work. Differences include the lack of a pyrrole methyl group on a fullerene derivative (which extends the π conjugation toward an acceptor), a reversal of the amide linker, and *para* versus *ortho* connectivity on an aryl linker, all of which have known effects on electronic current and charge transfer.[13,17]

Cheung et al. have approached computation of CT rates of the basic CPF (Figure 1) triad via the Fermi golden rule (FGR) expression.[18] They applied the linearized semiclassical approximation, developed by Geva,[19] which successfully reproduces experimental rate constants as long as the donor and acceptor potential energy surfaces are sufficiently harmonic. Under these assumptions, the FGR expression reduces to the Marcus expression via second-order cumulant approximation, and the parameters in the Marcus expression can be related to the dynamical statistics of the donor−acceptor energy band gap. With this approach and parametrization from molecular dynamics simulations with explicit solvent, their results indicate the formation of the first CT state at the picosecond scale and the second state at far longer times with little difference resulting from rigid or flexible triad nuclei. They further identify a fundamental amide mode (1700 cm^{-1}, C═O stretching) that is highly sensitive to the electronic state and triad conformation. This mode exhibits a blue shift of about 25 cm^{-1} between the $\pi-\pi^*$ and first CT states. Despite this sensitivity, there seems no imminent correlation between the mode position and the local electric field. Thereby, this mode is more likely to be sensitive to changes in the conjugations over other effects. With the dramatic shift in frequency, they propose that this mode can be probed to visualize or monitor the CT process.

This work presents a mixed quantum/molecular dynamics approach to simulating dynamics in highly conjugated organic systems. We eschew quantum mechanical treatment of all electrons for a significant reduction in computational cost and formulate an expression for the excited state in the reduced basis. Next we apply this prescription to simulate electron/nuclear relaxation dynamics which, for the systems under study, almost invariably produce a charge-transfer state. Finally, we approximate a charge-transfer rate from temporal analysis of excess charge, and we recover rates comparable to established experimental and theoretical values.

THEORETICAL METHODS

Electronic Dynamics. Characterizing the coupled electronic and nuclear dynamics in such systems can provide deep insight into the photophysical properties and may lead to the design of improved or novel materials for light-harvesting applications. However, given that modern quantum chemical techniques increase exponentially with system size, fully quantum simulations with correlated nuclear and electronic dynamics remain impossible for systems of any reasonable size without a profound loss of accuracy. Consequently, considerable effort has been made over many decades to develop approaches which compromise the fully quantum dynamics for computational efficiency. Each of these has distinct advantages, disadvantages, and pitfalls. Recent reviews of these methods can be found in refs 20 and 21.

In highly conjugated organic systems, the electronic properties of interest primarily happen within the closely packed π and π^* molecular orbitals. It is reasonable to assume that treating π-electrons quantum mechanically should sufficiently reproduce the charge-transfer dynamics while significantly reducing computational cost. The semiempirical Pariser−Parr−Pople (PPP)[22,23] model assumes negligible orbital overlap between σ- and π-states. This model, when parametrized carefully, provides a robust compromise between computational efficiency and an accurate representation of the electronic structure. Rossky and co-workers have made extensive use of this hybrid approach to highlight morphological and solvent characteristics which have a marked effect on electron/exciton dynamics. Such characteristics include side-chain effects on π-stacking and interchain energy migration,[24,25] solvent stabilization of nonradiative charge-transfer states,[26] and the influence of optical behavior by oligomer backbone twisting.[27]

Here, we employ the time-dependent Hartree−Fock (TDHF) approach and choose to evolve the density matrix in time via the Liouville−von Neumann equation[28]

$$i\hbar\frac{\partial\rho}{\partial t} = \langle[\mathcal{F}, \rho]\rangle = i\mathcal{L}\rho \tag{3}$$

where $\mathcal{F}$ is the Fock operator and the $\langle\cdots\rangle$ denotes a trace over the HF vacuum.[29] Formally, this is equivalent to performing a configuration-interaction (CI) calculation on a space of single excitations.[30] We expand the time propagator as a series of imaginary Chebyshev polynomials

$$(e^{-i\mathcal{L}dt})\rho(t) = \left(\sum_{k=0}^{N} a_k T_k(-i\mathcal{L}dt/R)\right)\rho(t) \tag{4}$$

where T_k is the k^{th} Chebyshev polynomial of the first kind. Each successive expansion term is recursively computable as

$$T_k(\hat{X}) = 2\hat{X}T_{k-1}(\hat{X}) + T_{k-2}(\hat{X}) \tag{5}$$

The Chebyshev expansion of the exponential is generally considered to be stable and converges rapidly. More importantly, this expansion scheme is norm preserving[31,32] which ensures that the trace of the density matrix ($\mathrm{Tr}[\rho]$ = number of electrons) is also preserved. All of these traits are highly beneficial for maintaining accuracy and stability during long-time propagation.

The Fock matrix is calculated at each time step based on the current nuclear geometry and the previous electronic density matrix.

$$\mathcal{F} = \mathcal{F}(\mathbf{R}(t + dt),\ \rho(t)) \tag{6}$$

The density matrix is propagated with the new Fock matrix, and force field parameters are adjusted based on new bond orders. The nuclei are iterated according to classical mechanics, and the iteration process repeats. At time $t = 0$, the ground-state SCF computation and CI excited states must still be computed; implementing the time evolution removes the need for subsequent diagonalizations. However, in practice, it is best to occasionally diagonalize the Fock matrix and collect the eigenspectrum to ensure that the Liouvillian superoperator remains within the limit where the Chebychev polynomials are defined.

Initialization and Excitation. The electronic structure calculation takes the following two considerations: (i) The system of study is spin-paired in the ground state. Thus, restricted Hartree−Fock (RHF) is applicable, and each state orbital $|\alpha\rangle$ has a corresponding and spatially identical state

https://dx.doi.org/10.1021/acs.jpcb.0c00202
J. Phys. Chem. B 2020, 124, 2149−2157

orbital $|\beta\rangle$. (ii) We consider only singlet excitations. As there are no spin flips, we need only to compute $|\alpha\rangle \rightarrow |\alpha\rangle$ transitions.

Naïvely, one may choose to prepare an excited state by elementary excitation, a simple promotion of an electron from an occupied state orbital to an unoccupied one. Doing so, however, fails to include coherences (off-diagonal elements in the density matrix). Both the Fock matrix and density matrix are diagonal in state representation, and in the context of the Liouville−von Neumann equation, no time evolution occurs.

$$i\hbar\frac{\partial\rho}{\partial t} = [\mathcal{F}^{(\text{state})}, \rho^{(\text{state})}] = 0$$

To prepare the system in an electronic excited state, we instead first define an electronic excitation operator

$$\hat{A}_n^{\dagger} = \sum_{p,h} z_{ph}^{*}\hat{\phi}_p^{\dagger}\hat{\phi}_h \tag{7}$$

that acts on the HF ground state to produce the n^{th} singly excited state and where z is the contribution of the elementary excitation from $h \rightarrow p$ for excitation n.

$$A_n^{\dagger}|HF\rangle = |n\rangle \tag{8}$$

Fermion operators $\hat{\phi}_i$ and $\hat{\phi}_j^{\dagger}$ remove or create electrons in the i or j HF molecular orbitals, and we denote h as the occupied ground-state orbitals and p as the unoccupied orbitals. The HF ground state is generated by populating the lowest-energy states from the vacuum state

$$|\text{HF}\rangle = \phi_1^{\dagger}...\phi_N^{\dagger}|0\rangle \tag{9}$$

for N number of electrons. The orbital operators $\hat{\phi}_k$ can be written as a linear combination of local atomic orbital operators, a_j

$$\phi_k^{\dagger} = \sum_j C_{jk}^{*}a_j^{\dagger} \tag{10}$$

Hence, matrix C is the unitary transform between the local (atomic) basis and the molecular orbital basis in which the Fock operator is diagonal. The ground-state density matrix is computed as

$$\rho_{\text{rs}} = \langle \text{HF}|a_{\text{s}}^{\dagger}a_{\text{r}}|\text{HF}\rangle \tag{11}$$

We now write the density matrix for singly excited state n in the same fashion.

$$\begin{aligned}\rho_{rs}^{(n)} &= \langle n|a_{\text{s}}^{\dagger}a_{\text{r}}|n\rangle \\ &= \sum_{ij}\langle n|\phi_i^{\dagger}\phi_h|n\rangle C_{si}^{*}C_{rj} \\ &= \sum_{ij}\sum_{p'h'}\sum_{ph} C_{si}^{*}C_{rj}z_{p'h}^{*}z_{ph} \times I_{php'h'}^{ij}\end{aligned} \tag{12}$$

Indices r and s correspond to site-local atomic orbitals; indices p and p' span over unoccupied molecular orbitals; indices h and h' span over occupied molecular orbitals in the ground state; and indices i and j span all molecular orbitals, occupied and unoccupied. The remaining term is given by

$$\begin{aligned}I_{php'h'}^{nm} &= \langle \text{HF}|\phi_h^{\dagger}\phi_p,\phi_n^{\dagger}\phi_m\phi_p^{\dagger}\phi_h|\text{HF}\rangle \\ &= \delta_{hh'}\delta_{np'}\delta_{mp} - \delta_{pp'}\delta_{mh}\delta_{nh} \\ &+ \delta_{pp'}\delta_{hh'}\delta_{n_{\text{occ}},m_{\text{occ}}}\end{aligned} \tag{13}$$

where h, h', p, p', m, and n iterate through the molecular orbitals, taken as eigenvectors of the Fock operator. We examine these terms independently to interpret their physical meaning. The first term is nonzero for m and n corresponding to unoccupied orbitals and adds magnitude to the population and coherence terms (particle). The second term is nonzero for m and n corresponding to occupied orbitals and subtracts magnitude (hole). The third term accounts for the otherwise unaffected populations of the ground state.

Nuclear−Electronic Coupling. The density matrix ρ, in site basis, can be interpreted as the bond-change matrix where the diagonal matrix elements ρ_{ii} correspond to the occupation of local orbital i, and the off-diagonal terms ρ_{ij} correspond to the density shared by local orbitals i and j. Off-diagonal elements for bonded atoms i and j represent the π-bond order between these atoms. Changes in the electronic density matrix correspond to changes in the local electronic population and π-bond order between connected atoms. With this in mind, we make the assumption that the MM3 force-field parameters[33] as implemented in TINKER molecular dynamics code[34] can be expressed as linear functions of the bond-charge matrix and that this interpolation can be used to describe the force field for both the ground and low-lying $\pi \rightarrow \pi^*$ excitations of the system, including charge-separated and charge-transfer states. The equilibrium bond length between pairs of bonded atoms is calculated using a linear interpolation between single and double bond lengths. Thus, for bonded atoms i and j, the equilibrium bond length is

$$r_{ij} = r_{ij}^0 + \delta r_{ij}(1 - \rho_{ij}) \tag{14}$$

where r_{ij}^0 is the bond length for a full double bond (with $\rho_{ij} = 1$). Similarly, the bond force constants and torsional barriers are interpolated as

$$k_{ij} = k_{ij}^0 - \delta k_{ij}(1 - \rho_{ij}) \tag{15}$$

$$t_{ij} = \rho_{ij}t_{ij}^0 \tag{16}$$

Clearly, an increase in the bond order (π-bond character) results in decreases in equilibrium length and increases in bond force constant and torsional barrier. Under these assumptions, the nuclear degrees of freedom evolve with the π-electronic density matrix rather than on a single Born−Oppenheimer surface as per the Ehrenfest approximation. This approximation is certainly justified for large systems with a high density of states where surface hopping methods are known to be problematic.[35,36] In general, off-diagonal elements of the density matrix have nonzero imaginary value, whereas the above parameter interpolations require a real-valued input. The sign of $Re[\rho_{i,j}]$ describes whether the interaction between two atoms is bonding or antibonding in character.[37] To preserve this description, we compute the parameters from the real-valued part of the density matrix.

RESULTS

We are interested in studying the charge-transfer properties of four DBA triad systems studied by Moore and co-workers.[6,9]

https://dx.doi.org/10.1021/acs.jpcb.0c00202
J. Phys. Chem. B 2020, 124, 2149−2157

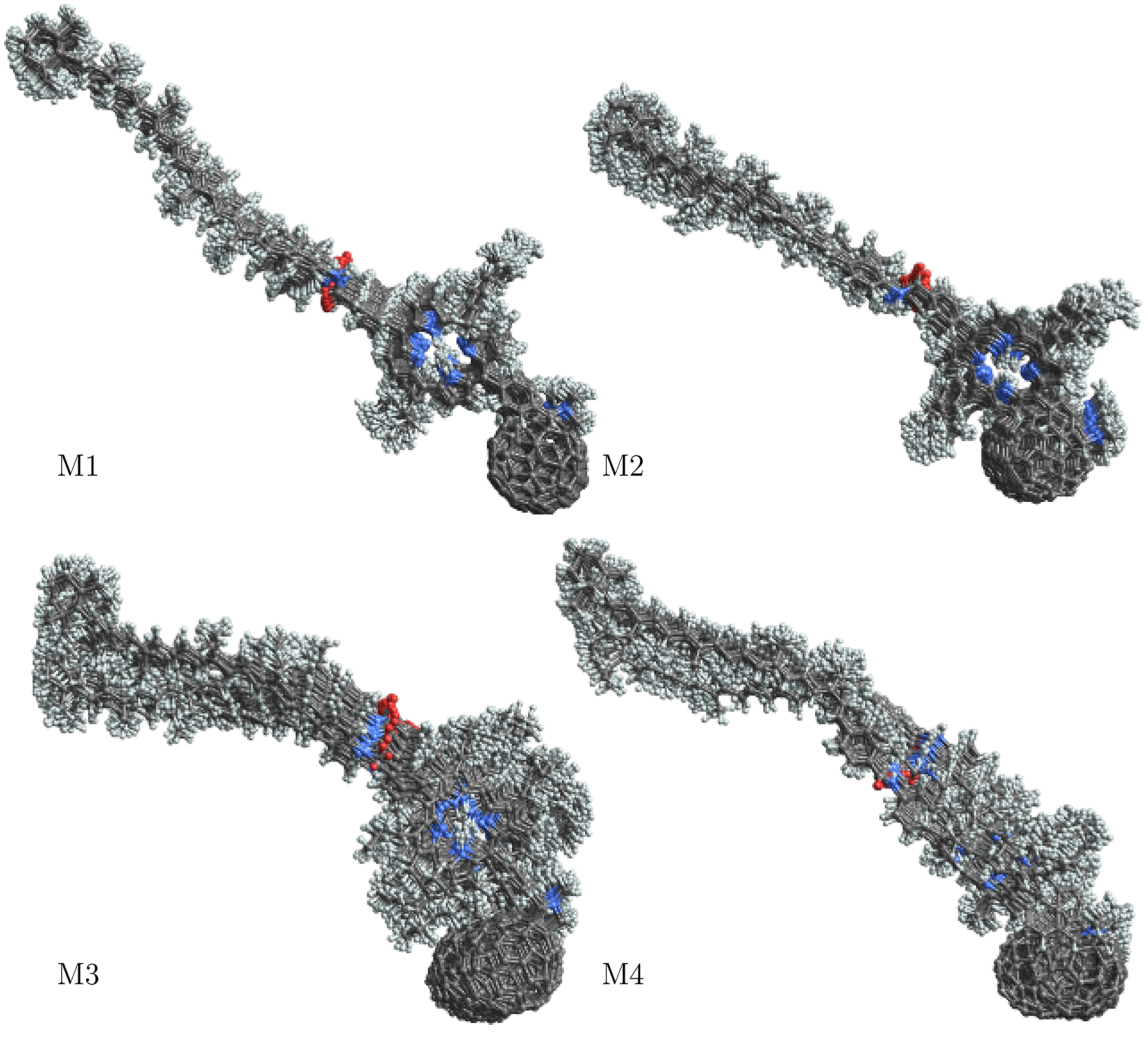

Figure 2. Overlay of starting geometries for molecules **M1**−**M4**.

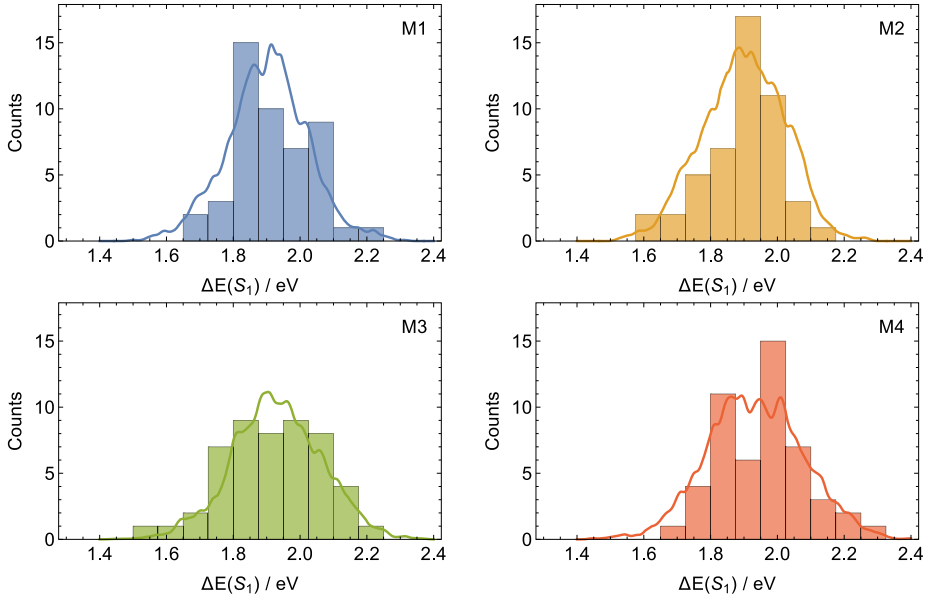

Figure 3. Energy distributions for the first excited singlet state for each molecule. Smooth distributions represent the distribution of excitation energies from 5000 ground state samplings each. Discrete histograms represent the 50 initial configurations chosen for the ensemble.

https://dx.doi.org/10.1021/acs.jpcb.0c00202
J. Phys. Chem. B 2020, 124, 2149−2157

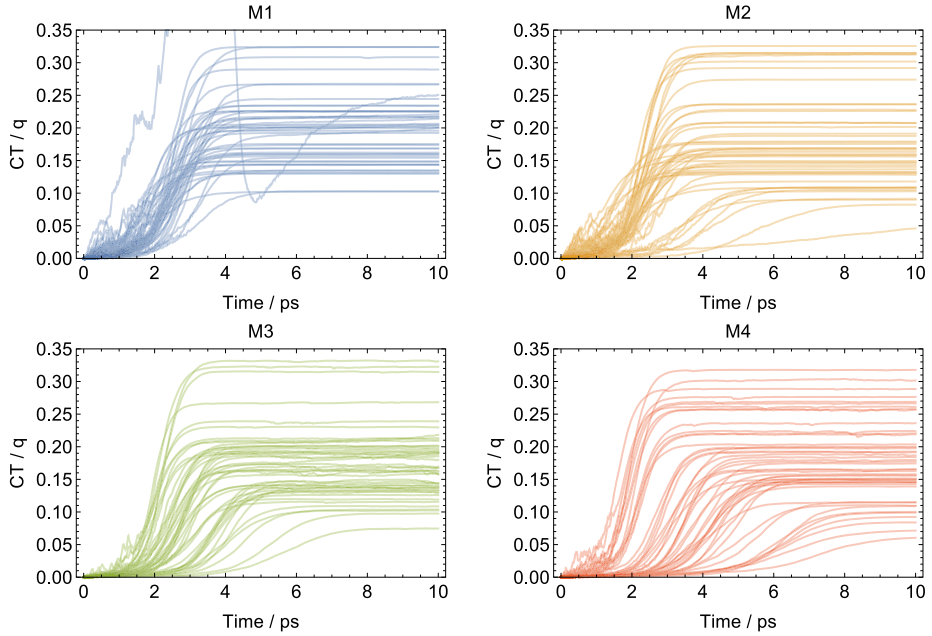

Figure 4. Charge accumulation plots for each trajectory. Plots generally follow a logistic growth regression excluding one anomalous trajectory in **M1**.

Figure 1 shows the breakdown of each molecule. Each molecule has the same acceptor (C_{60} derivative) and polymeric donor (carotenoid) and is differentiated by their side groups on porphyrin bridges. In Molecule 1 (**M1**), the porphyrin ring is dressed by trisubstituted aryl groups. Molecule 2 (**M2**) is identical to **M1** except for the two methyl substitutions on the aryl groups. Molecule 3 (**M3**) has methyl and *n*-butyl groups on the pyrrole sites. Molecule 4 (**M4**), similar to **M3**, replaces the longer chain with ethyl groups (Figure 2). Additionally, the amide group is reversed on **M4** relative to those of **M1**−**3**. The four molecules were constructed and preoptimized using external software, AVOGADRO.[38] Each structure was thermalized with a Nosé−Hoover thermostat set to T = 300 K (operational temperature) in vacuum for 10 ps at a time step of 0.01 fs (10^6 time steps). Our simulations here are done in vacuum with the expressed intent to focus specifically on the role of internal molecular degrees of freedom in charge-transfer dynamics. The time step must be chosen to capture electron dynamics adequately and should be shorter than the oscillation period of the time evolution operator. We therefore want $\delta t < \hbar/E$ or $E < \hbar/\delta t$, and our choice allows for the Liouvillian eigenspectrum to range between ±1.2 hartree.

Thermal fluctuations in the molecular configuration modulate the excitation energy, and we need to check that the distribution of excitation energies of our initial geometries matches that of the full configurational space. We assume that in the last 5 ps of the ground-state dynamics each system samples operational temperature configurations and that a selection of 5000 geometries adequately represents the full configurational space. Figure 3 compares the energy distributions of the selected initial geometries and subset of 5000 geometries. We find that the excitation energies match the distribution of the broader configuration space and that the average excitation energies also are in good agreement with experimental absorption spectra of the lowest excitation energy for the porphyrin moieties (∼1.9 eV).[6,9]

We sample 50 geometries (every 100 fs) as the basis for the ensemble. (Note that we retain the coordinates and velocities of each sample.) We perform a single-point calculation on each of these samples to determine the correct excited state to choose. For these triads, the excitation should resemble an exciton localized to the porphyrin bridge. We determine the correct excitation using the eigenvectors of the Fock and CI matrices in the following way. Let $C_{i,j}$ be the contribution of atomic orbital i to molecular orbital j and z^n_{hp} be the contribution of elementary excitation (from molecular orbital h to p) to the n^{th} excited state. Then, for any CI excitation, N, we calculate the percentage of the hole density localized to the bridge as

$$P_{\text{hole}}(n) = \sum_{i\in\text{Brg}} \sum_{h\in\text{occ}} |C_{i,h}|^2 \, |z^n_h|^2 \tag{17}$$

where i sums over atoms in the bridge moiety and h over the occupied molecular orbitals. Correspondingly, the percentage of electron density can be calculated as

$$P_{\text{elec}}(n) = \sum_{i\in\text{Brg}} \sum_{p\in\text{unocc}} |C_{i,p}|^2 \, |z^n_p|^2 \tag{18}$$

for p over the unoccupied molecular orbitals. We choose the lowest-energy excitation which has P_{hole} and P_{elec} larger than 0.75 (at least 75% of the exciton density is localized to the bridge). For most configurations, this corresponds to the first excited state (≈2.0 eV). Each geometry is excited at t = 0 and then freely relaxes given an energy kick for 10 ps. Other simulation parameters are kept consistent with the thermalization procedure. This recreates the scenario of a molecule undergoing thermal fluctuations at operational temperatures, becoming photoexcited, and then undergoing electronic and nuclear relaxation.

Rate Approximation. The diagonal terms of the density matrix (bond-charge matrix) give the occupation number for an orbital. Thus, in the site basis, ρ_{ii} represents an electron count on orbital i centered on some π-active nucleus. Then, a partial trace of the density matrix, choosing for atoms assigned to a particular moiety, accounts for the total number of

https://dx.doi.org/10.1021/acs.jpcb.0c00202
J. Phys. Chem. B 2020, 124, 2149−2157

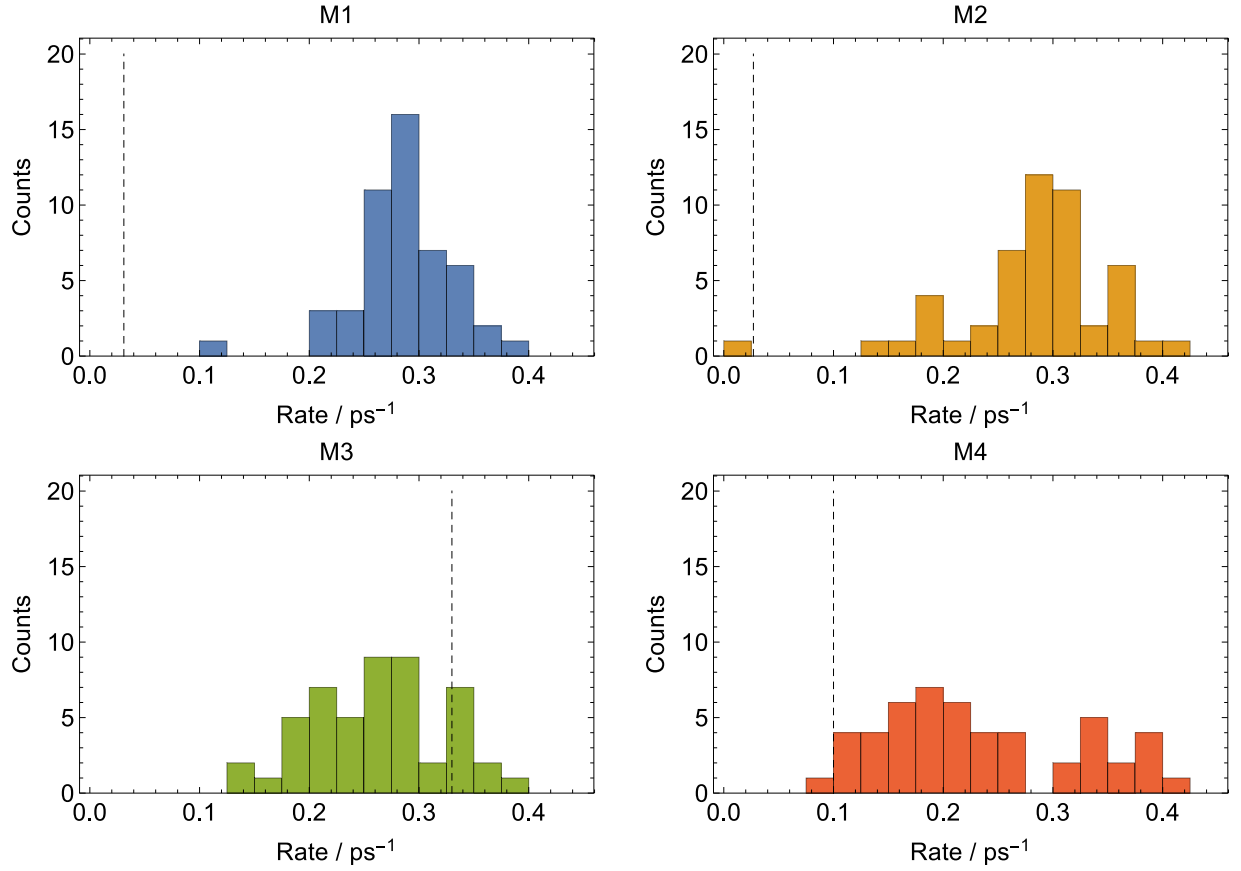

Figure 5. Histogram of the charge-transfer rates of each ensemble. Averaged rates for **M1−4** are 0.28 ± 0.04 ps^{-1}, 0.28 ± 0.07 ps^{-1}, 0.26 ± 0.06 ps^{-1}, and 0.23 ± 0.06 ps^{-1}, respectively. Dashed lines indicate experimentally reported values with rate for **M4** reported as a maximum.[9]

electrons localized to that moiety; the full trace of the density matrix reflects the total electron count of the system. The effective charge (population gain) is this partial trace of the density matrix at time t subtracted by the ground-state charge. For the acceptor moiety

$$q_{\mathrm{acc}}(t) = \sum_{i \in \mathrm{acc}} (\rho_{ii}(t) - \rho_{ii}^{\mathrm{gs}}) \tag{19}$$

For multimolecular systems, this calculation can be extended to consider charging of whole molecules. We measure charge transfer by following the excess population in acceptor moiety in time for each trajectory. Fitting the charge-transfer plots from each trajectory to a logistic growth function provides an approximate form

$$q(t) = \frac{q_{\max}}{1 + \exp[-k(t - t_c)]} + q_0 \tag{20}$$

where $q_{\max}$ is the long-time maximal charge transferred; k is a steepness factor; t_c is the function center (50% completion time); and q_0 is an initial charge amount. Nonzero q_0 represents some partial charge-transfer character in the initial excited state. From these regressions, the fractional completion time can be computed as

$$t_\alpha = t_0 + \frac{1}{k} \ln\left[\frac{\alpha}{1 - \alpha}\right] \tag{21}$$

We take the 95% (α = 0.95) completion time to represent a charge-transfer time scale; the inverse of t_α is interpreted as the reaction rate.

Figure 4 plots the excess electron charge transferred to the C_{60} moieties for each trajectory. Following t = 0 excitation, most trajectories do not immediately begin the CT process. Some chaotic behavior occurs in the early time, which can be interpreted as the system responding to a vertical excitation, before settling into a smooth charge-transfer regime. Finally, when CT has completed (reached a maximum), the charge separation is stable and long lived. We have not evolved the trajectories past 10 ps; formation of the second charge-transfer state (C^+−P−C_{60}^-) is on the order of multiple tens to hundreds of picoseconds with a lifetime into the nanosecond scale.[9]

All four molecules successfully undergo some amount of charge transfer within 10 ps. This implies that charge transfer itself is determined by the offset between HOMO and LUMO energy levels of the donor and acceptor moieties. Additionally, it agrees with experimentally observed quantum yield of unity. However, the amount and rate of CT depend on the finer details of the molecular structure. We see the range of total charge transferred, between 0.05 and 0.35q, is consistent through all molecules, while the distributions of the CT curves differ among them.

Charge accumulation follows a logistic growth function quite well (R^2 > 0.99), excluding one errant trajectory in **M1**. Further investigation of this simulation shows the lowest-energy porphyrin excitation of ∼3 eV, producing an extremely "hot" excition. This excitation is anomalously high compared to the 1.9 eV for all other trajectories. Therefore, we deem this a significant outlier and exclude it from further analysis. We approximate rate constant as the inverse of the 95% completion time (using the logistic fits which are plotted).

https://dx.doi.org/10.1021/acs.jpcb.0c00202
J. Phys. Chem. B 2020, 124, 2149−2157

Table 1. Comparison of CP*F → CP$^+$F$^-$ Transition Rates in ps^{-1} for Various Systems As Computed Using Various Approximations and Methods[a]

method	M1	M2	M3	M4	note
Marcus rate (linear)			0.01		ref 39
Marcus rate (bent)			0.34		ref 39
Marcus rate (bent/flexible)			0.30 ± 0.02		ref 18
Marcus rate (bent/rigid)			0.36 ± 0.07		ref 18
LSC (bend/flexible)			0.29 ± 0.02		ref 18
LSC (bend/rigid)			0.39 ± 0.07		ref 18
TDDFT/LDA (linear/dynamic)		≈14 ps^{-1} (70 fs)			ref 15
TDDFT/LDA (all clamped)		no transfer			ref 15
MD/TDHF	0.28 ± 0.04	0.28 ± 0.07	0.26 ± 0.06	0.23 ± 0.06	this work
exptl	0.0310	0.0270	0.3300	≤0.1000	refs 8 and 9

[a]The "Marcus" rates are reported using the classical Marcus expression as parameterized from simulation. LSC = linearized semiclassical method developed by Geva and co-workers (refs 18 and 19). Note that in ref 15 the authors report simulations on a triad lacking the diaryl groups and with a conjugated link between the porphyrin and fullerene.

Figure 5 adds crucial information about the CT rates, which are difficult to assess from the multitude of trajectories in Figure 4. From Figure 5, we can clearly see that the differences in chemical structure, even subtle ones, alter CT rates and their distribution. Table 1 provides a summary of CP*F → CP$^+$F$^-$ transition rates reported using various theoretical approaches as well as the experimental rates reported in ref 9. Our results compare favorably against previously reported experimental and theoretical results for the **M3** system. While our approach overestimates rates for **M1** and **M2** as compared to experiment, the rates for **M3** and **M4** are in good agreement with experimental results.[9] However, the overestimation is systematic between the pair of molecules, and we are able to reproduce the relative rates observed in the experiment.

Interestingly, trajectories which take the longest to begin the charge-transfer process tend to have a proportionately less total charge transferred. **M2−4** have prominent examples of such where CT does not begin until about 4 ps and ultimately settles at a 0.1 q of charge transferred. This is a long enough time frame to where the bridge nuclei could have responded to the electronic excitation and rearranged to more stably house the exciton. Either the driving force for charge transfer is mitigated or the new configuration/electronic structure has less charge-transfer character.

CONCLUSIONS

We have presented here the results of mixed quantum mechanical/molecular mechanics simulations modeling electron and nuclear dynamics in four donor−bridge−acceptor triads, each with slightly differing bridge constructions. By taking a statistical approach, we ensure our simulations are representative of the average charge-transfer behavior of these systems. Our model can reproduce experimentally accurate excitation energies for a localized excitation on the porphyrin bridge. Electron population analysis indicates that the initial charge transfer from the porphyrin bridge to the fullerene acceptor occurs at the picosecond scale. While we systematically overestimate charge-transfer rates in **M1** and **M2**, we reasonably reproduces rates in **M3** and **M4** when compared to experimental findings.[9]

Our method achieves rapid electronic dynamics simulations by focusing quantum treatment on only π-electrons and relegating σ-electrons to force fields. Mapping the excess charge accumulation on the acceptor to a logistic function provides an approximation to the charge-transfer rate. Thus, this method provides a computationally inexpensive method for computing such reaction rates in conjugated polymers. Furthermore, rapid computation and analysis allow for more efficient sampling and identification of more efficient charge-transfer systems.

We acknowledge our findings here result from gas-phase simulations, whereas previous experimental and theoretical works indicate strong solvent influence on the charge-transfer character of such molecules. While we do recognize the marked effects of a polar environment, we present here an initial step in the development of our framework. Vacuum simulations provide a description of uninhibited nuclear dynamics occurring during the CT process. Inclusion of explicit solvent molecules in further simulations will allow for a direct comparison, thus highlighting any effects pertaining to CT state stabilization, molecular conformations, or vibrational energy dissipation of the triads.

In the accompanying paper, we analyze the nuclear dynamics and provide a time-resolved vibrational power spectrum characterizing the nuclear vibrations occurring in our simulations and identify a number of vibrational modes crucial to the charge-transfer process.

AUTHOR INFORMATION

Corresponding Author

Eric R. Bittner − *Department of Chemistry, University of Houston, Houston, Texas 77204, United States; Department of Physics, Durham University, Durham DH1 3LE, United Kingdom;* orcid.org/0000-0002-0775-9664; Email: ebittner@central.uh.edu

Author

Kush Patel − *Department of Chemistry, University of Houston, Houston, Texas 77204, United States;* orcid.org/0000-0003-0485-9982

Complete contact information is available at: https://pubs.acs.org/10.1021/acs.jpcb.0c00202

Notes

The authors declare no competing financial interest.

ACKNOWLEDGMENTS

The work at the University of Houston was funded in part by the National Science Foundation (CHE-1664971, MRI-1531814) and the Robert A. Welch Foundation (E-1337).

https://dx.doi.org/10.1021/acs.jpcb.0c00202
J. Phys. Chem. B 2020, 124, 2149−2157

E.R.B. acknowledges the Leverhulme Trust for support at Durham University.

REFERENCES

(1) Gust, D.; Moore, T. A.; Liddell, P. A.; Nemeth, G. A.; Makings, L. R.; Moore, A. L.; Barrett, D.; Pessiki, P. J.; Bensasson, R. V. Charge Separation in Carotenoporphyrin-Quinone Triads: Synthetic, Conformational, and Fluorescence Lifetime Studies. *J. Am. Chem. Soc.* **1987**, *109*, 846−856.

(2) Macpherson, A. N.; Liddell, P. A.; Lin, S.; Noss, L.; Seely, G. R.; DeGraziano, J. M.; Moore, A. L.; Moore, T. A.; Gust, D. Ultrafast Photoinduced Electron Transfer in Rigid Porphyrin−Quinone Dyads. *J. Am. Chem. Soc.* **1995**, *117*, 7202−7212.

(3) Kuciauskas, D.; Lin, S.; Seely, G. R.; Moore, A. L.; Moore, T. A.; Gust, D.; Drovetskaya, T.; Reed, C. A.; Boyd, P. D. Energy and Photoinduced Electron Transfer in Porphyrin-Fullerene Dyads. *J. Phys. Chem.* **1996**, *100*, 15926−15932.

(4) Liddell, P. A.; Kuciauskas, D.; Sumida, J. P.; Nash, B.; Nguyen, D.; Moore, A. L.; Moore, T. A.; Gust, D. Photoinduced Charge Separation and Charge Recombination to a Triplet State in a Carotene-Porphyrin-Fullerene Triad. *J. Am. Chem. Soc.* **1997**, *119*, 1400−1405.

(5) Bahr, J. L.; Kuciauskas, D.; Liddell, P. A.; Moore, A. L.; Moore, T. A.; Gust, D. Driving Force and Electronic Coupling Effects on Photoinduced Electron Transfer in a Fullerene-based Molecular Triad. *Photochem. Photobiol.* **2000**, *72*, 598−611.

(6) Kuciauskas, D.; Liddell, P. A.; Lin, S.; Stone, S. G.; Moore, A. L.; Moore, T. A.; Gust, D. Photoinduced Electron Transfer in Carotenoporphyrin-Fullerene Triads: Temperature and Solvent Effects. *J. Phys. Chem. B* **2000**, *104*, 4307−4321.

(7) Gust, D.; Moore, T. A.; Moore, A. L. Mimicking Photosynthetic Solar Energy Transduction. *Acc. Chem. Res.* **2001**, *34*, 40−48.

(8) Smirnov, S. N.; Liddell, P. A.; Vlassiouk, I. V.; Teslja, A.; Kuciauskas, D.; Braun, C. L.; Moore, A. L.; Moore, T. A.; Gust, D. Characterization of the Giant Transient Dipole Generated by Photoinduced Electron Transfer in a Carotene-Porphyrin-Fullerene Molecular Triad. *J. Phys. Chem. A* **2003**, *107*, 7567−7573.

(9) Kodis, G.; Liddell, P. A.; Moore, A. L.; Moore, T. A.; Gust, D. Synthesis and Photochemistry of a Carotene−Porphyrin−Fullerene Model Photosynthetic Reaction Center. *J. Phys. Org. Chem.* **2004**, *17*, 724−734.

(10) Kuciauskas, D.; Liddell, P. A.; Hung, S.-C.; Lin, S.; Stone, S.; Seely, G. R.; Moore, A. L.; Moore, T. A.; Gust, D. Structural Effects on Photoinduced Electron Transfer in Carotenoid-Porphyrin-Quinone Triads. *J. Phys. Chem. B* **1997**, *101*, 429−440.

(11) Carbonera, D.; Di Valentin, M.; Corvaja, C.; Agostini, G.; Giacometti, G.; Liddell, P. A.; Kuciauskas, D.; Moore, A. L.; Moore, T. A.; Gust, D. EPR Investigation of Photoinduced Radical Pair Formation and Decay to a Triplet State in a Carotene-Porphyrin-Fullerene Triad. *J. Am. Chem. Soc.* **1998**, *120*, 4398−4405.

(12) Aviram, A.; Ratner, M. A. Molecular Rectifiers. *Chem. Phys. Lett.* **1974**, *29*, 277−283.

(13) Ding, W.; Negre, C. F. A.; Vogt, L.; Batista, V. S. Single Molecule Rectification Induced by the Asymmetry of a Single Frontier Orbital. *J. Chem. Theory Comput.* **2014**, *10*, 3393−3400.

(14) Metzger, R. M. Unimolecular Electrical Rectifiers. *Chem. Rev.* **2003**, *103*, 3803−3834.

(15) Andrea Rozzi, C.; Maria Falke, S.; Spallanzani, N.; Rubio, A.; Molinari, E.; Brida, D.; Maiuri, M.; Cerullo, G.; Schramm, H.; Christoffers, J.; Lienau, C.; et al. Quantum Coherence Controls the Charge Separation in a Prototypical Artificial Light-Harvesting System. *Nat. Commun.* **2013**, *4*, 1602−1608.

(16) Marques, M. Octopus: A First-Principles Tool for Excited Electron-Ion Dynamics. *Comput. Phys. Commun.* **2003**, *151*, 60−78.

(17) Manrique, D. Z.; Huang, C.; Baghernejad, M.; Zhao, X.; Al-Owaedi, O. A.; Sadeghi, H.; Kaliginedi, V.; Hong, W.; Gulcur, M.; Wandlowski, T.; Bryce, M. R.; Lambert, C. J.; et al. A Quantum Circuit Rule for Interference Effects in Single-Molecule Electrical Junctions. *Nat. Commun.* **2015**, *6*, 1−8.

(18) Sun, X.; Zhang, P.; Lai, Y.; Williams, K. L.; Cheung, M. S.; Dunietz, B. D.; Geva, E. Computational Study of Charge-Transfer Dynamics in the Carotenoid-Porphyrin-C60 Molecular Triad Solvated in Explicit Tetrahydrofuran and its Spectroscopic Signature. *J. Phys. Chem. C* **2018**, *122*, 11288−11299.

(19) Shi, Q.; Geva, E. Nonradiative Electronic Relaxation Rate Constants from Approximations Based on Linearizing the Path-Integral Forward-Backward Action. *J. Phys. Chem. A* **2004**, *108*, 6109−6116.

(20) Nelson, T.; Fernandez-Alberti, S.; Roitberg, A. E.; Tretiak, S. Nonadiabatic Excited-State Molecular Dynamics: Modeling Photophysics in Organic Conjugated Materials. *Acc. Chem. Res.* **2014**, *47*, 1155−1164.

(21) Curchod, B. F. E.; Martínez, T. J. Ab Initio Nonadiabatic Quantum Molecular Dynamics. *Chem. Rev.* **2018**, *118*, 3305−3336.

(22) Pariser, R.; Parr, R. G. A Semi-Empirical Theory of the Electronic Spectra and Electronic Structure of Complex Unsaturated Molecules. II. *J. Chem. Phys.* **1953**, *21*, 767−776.

(23) Pople, J. A. Electron Interaction in Unsaturated Hydrocarbons. *Trans. Faraday Soc.* **1953**, *49*, 1375−1385.

(24) Sterpone, F.; Bedard-Hearn, M. J.; Rossky, P. J. Nonadiabatic Mixed Quantum-Classical Dynamic Simulation of π-Stacked Oligophenylenevinylenes. *J. Phys. Chem. A* **2009**, *113*, 3427−3430.

(25) Hu, Z.; Adachi, T.; Haws, R.; Shuang, B.; Ono, R. J.; Bielawski, C. W.; Landes, C. F.; Rossky, P. J.; Vanden Bout, D. A. Excitonic Energy Migration in Conjugated Polymers: The Critical Role of Interchain Morphology. *J. Am. Chem. Soc.* **2014**, *136*, 16023−16031.

(26) Hu, Z.; Willard, A. P.; Ono, R. J.; Bielawski, C. W.; Rossky, P. J.; Vanden Bout, D. A. An Insight into Non-Emissive Excited States in Conjugated Polymers. *Nat. Commun.* **2015**, *6*, 8246.

(27) Simine, L.; Rossky, P. J. Relating Chromophoric and Structural Disorder in Conjugated Polymers. *J. Phys. Chem. Lett.* **2017**, *8*, 1752−1756.

(28) Schatz, G. C.; Ratner, M. A. *Quantum Mechanics in Chemistry (Dover Books on Chemistry)*; Dover Publications, 2002.

(29) Blaizot, J. P.; Ripka, G. *Quantum Theory of Finite Systems*; The MIT Press: Cambridge, MA, 1986.

(30) Tretiak, S.; Mukamel, S. Density Matrix Analysis and Simulation of Electronic Excitations in Conjugated and Aggregated Molecules. *Chem. Rev.* **2002**, *102*, 3171−3212.

(31) Tal-Ezer, H.; Kosloff, R. An Accurate and Efficient Scheme for Propagating the Time Dependent Schrodinger Equation. *J. Chem. Phys.* **1984**, *81*, 3967−3971.

(32) Kosloff, R. Time-Dependent Quantum-Mechanical Methods for Molecular Dynamics. *J. Phys. Chem.* **1988**, *92*, 2087−2100.

(33) Allinger, N. L.; Yuh, Y. H.; Lii, J. H. Molecular Mechanics. The MM3 Force Field for Hydrocarbons. 1. *J. Am. Chem. Soc.* **1989**, *111*, 8551−8566.

(34) Ponder, J. W.; Richards, F. M. An Efficient Newton-like Method for Molecular Mechanics Energy Minimization of Large Molecules. *J. Comput. Chem.* **1987**, *8*, 1016−1024.

(35) Tully, J. C. Molecular Dynamics with Electronic Transitions. *J. Chem. Phys.* **1990**, *93*, 1061−1071.

(36) Granucci, G.; Persico, M. Critical Appraisal of the Fewest Switches Algorithm for Surface Hopping. *J. Chem. Phys.* **2007**, *126*, 134114.

(37) Pople, J. A.; Segal, G. A. Approximate Self-Consistent Molecular Orbital Theory. II. Calculations with Complete Neglect of Differential Overlap. *J. Chem. Phys.* **1965**, *43*, S136−S151.

(38) Hanwell, M. D.; Curtis, D. E.; Lonie, D. C.; Vandermeersch, T.; Zurek, E.; Hutchison, G. R. Avogadro: An Advanced Semantic Chemical Editor, Visualization, and Analysis Platform. *J. Cheminf.* **2012**, *4*, 17.

(39) Manna, A. K.; Balamurugan, D.; Cheung, M. S.; Dunietz, B. D. Unraveling the Mechanism of Photoinduced Charge Transfer in Carotenoid-Porphyrin-C60 Molecular Triad. *J. Phys. Chem. Lett.* **2015**, *6*, 1231−1237.

https://dx.doi.org/10.1021/acs.jpcb.0c00202
J. Phys. Chem. B 2020, 124, 2149−2157